RESEARCH ARTICLE

Surface Modification of PAN-Derived Commercial Graphite Felts Using Deep Eutectic Solvents for their Application as Electrodes in All-Vanadium Redox Flow Batteries

L. Mauricio Murillo-Herrera[a], Eneith S. Aguilar[a], Michael W. Thielke[a] and Ana Jorge Sobrido*[a]

[a] Dr L. M. Murillo-Herrera, E. S. Aguilar, Dr M. W. Thielke, Dr A. Jorge Sobrido
Department School of Engineering and Materials Science
Institution: Queen Mary University of London
Address: Mile End Rd, Bethnal Green, London E1 4NS, United Kingdom
E-mail: a.sobrido@qmul.ac.uk

Supporting information for this article is given via a link at the end of the document.

Abstract: All-vanadium redox flow batteries are promising large-scale energy storage solutions to support intermittent power generation. Commercial graphite felts are among the most used materials as electrodes for these batteries due to their cheap price, high conductivity, and large surface area. However, these materials exhibit poor wettability and electrochemical activity towards vanadium redox reactions, which translates into overpotentials and lower efficiencies. Deep eutectic solvents (DES) are mixtures of Lewis acids and bases that exhibit lower melting points than their original components. Here, a DES composed of choline chloride and urea, and a DES composed of $FeCl_3$ and NH_4Cl have been employed to modify the surface of graphite felts alongside a series of re-carbonization steps. The resulting materials were compared against pristine, thermally activated, and oxidatively activated graphite felts. Our results indicated that the treatments introduced new oxygen and nitrogen functionalities to the carbonaceous surface and increased the surface area, the degree of disorder and defects in the graphitic layers of the fibres. Cyclic voltammetry studies demonstrated higher electrochemical activity towards vanadium redox reactions and electrochemical impedance spectroscopy experiments showed the modified materials exhibited significantly lower charge transfer resistances. When tested in full cell configuration the electrode modified with the urea-based DES exhibited comparable coulombic efficiencies and superior energy storage capacity retention than the thermally oxidized felt used as benchmark, suggesting that the introduction of oxygen- and nitrogen-rich functional groups had a positive effect on the overall electrochemical performance of graphite felts.

Introduction

The growing climate change and global warming have made it necessary to reduce our dependence on fossil fuels and have accelerated the development of renewable energy sources, especially the use of wind and solar power. Next to energy harvesting, the role of energy storage is just as important to level out the fluctuating nature of these renewable energy resources and to ensure the electrical grid can cover the demand at any time.

One of the most promising technologies emerging in the field of stationary energy storage systems are redox flow batteries (RFBs), due to their decoupled storage system for power and energy that allows increasing the energy capacity through upscaling the size and concentration of the electrolyte tanks, while the power is dependent on the active species and the electrode size. One unique feature of RFBs is that the electrochemically active species are continuously pumped through half-cells as the anolyte and catholyte, separated from each other by an ion-exchange membrane with each in contact with the electrically conductive electrode. All-vanadium RFBs (VRFB) have increasingly attracted more interest due to their longevity, high reliability, and low operation and maintenance costs.[1] The VRF stores energy through the redox reactions of VO_2^+ / VO^{2+} in the catholyte and V^{2+} / V^{3+} in the anolyte. The use of vanadium species in both anolyte and catholyte minimizes the crossover effect, a common cause of failure and decrease in performance of RFBs.[2]

Electrodes in RFBs are one of the key components and an important factor in promoting higher performance, durability, and lifetime, and therefore determining costs and commercial applicability.[3] The electrodes need to fulfil specific criteria to mechanically withstand the constant flow of electrolyte, while providing a high electrochemically active surface area that interacts well with the aqueous electrolytes through a suitable wettability to kinetically generate a high rate of reactions, without lowering the pressure or blocking the constant flow. Next to these properties, electric conductivity, (electro)chemical inertness, and catalytic activity are important parameters of electrodes in batteries. The redox reactions of both vanadium redox pairs occur on the surface of the electrode. Therefore polarization resistance induced by the redox reactions directly affects the overall performance, and strongly depends on the physicochemical properties of the electrodes.[4] The most employed electrodes for redox flow batteries are based on carbon fibres, such as graphitic felts (GF)[5], while electrospun fibres are gaining more and more interest as an alternative[6]. Carbon electrodes are usually synthesized by carbonization of polyacrylonitrile (PAN).[3b] However, commercial GFs perform poorly, exhibiting relatively low activity toward the redox reactions of vanadium, due to lack of reactive sites and hydrophobic surface properties.[7] Different approaches have been reported to improve the properties of the electrodes based on surface modification through heteroatom doping or catalyst deposition.[8] A typical method to enhance the properties of GFs / papers involves a thermal treatment by which the electrode surface is oxidized in an air at 400 °C for 30 h for graphite felts and 475 °C for carbon papers.[9] Other methods based on chemical modification of the surface have been reported to induce heteroatom functionalities, such as nitrogen[10] or phosphorus[7] that promote the interaction with vanadium ions through built-in defects at the fibre surface. Other methods to further improve the performance of the carbons include addition of precious metallic[11] or metal oxide nanoparticles[12], addition of carbon nanoparticles[13], or biomass-derived carbon particles[14], which extend the existing surface and add catalytic functionalities for redox reactions onto the GF.

The use of ionic liquids has generated growing interest in the last decades due to their unique properties, such as negligible vapour pressure, non-flammability, high heat capacity, good solubility for ionic compounds, immiscibility with most organic solvents, potential for reutilization and design flexibility.[15] Because of this, they have been proposed as sustainable candidates to substitute

commercial solvents, yet their commercial use has been limited due to their high cost and non-environmentally friendly syntheses.[16] Deep eutectic solvents (DESs) are binary or tertiary mixtures of Lewis acids and bases. When these components are mixed at specific molar fractions, the resulting mixture exhibits a steep decrease in its melting point, far lower than each of the constituents. DESs are analogous to ionic liquids since they contain a high proportion of ions but, unlike ionic liquids, DESs are not purely ionic compounds. Due to their simple synthesis, the production of DESs is significantly cheaper and more sustainable than ionic liquids.[17]

DESs can be classified into four categories according to the nature of their components. Type I is composed of ammonium, phosphonium or sulphonium halides and transition metal halides, such as $AlCl_3$ or $SnCl_2$. Type II is an extension of type I to hydrated metal halides such as $FeCl_3O6H_2O$ or $CoCl_2O6H_2O$. Type III is composed of the same ammonium, phosphonium or sulphonium salts and hydrogen-bond donors like polyols, amines, amides, or organic acids. Type IV consists of metal halides and hydrogen-bond donors.[17] DESs have found applications in the synthesis and modification of carbonaceous. Hayyan *et al*. reported the functionalization of graphene and carbon nanotubes with a variety of type III DESs, with polyols, amides and organic acids as hydrogen-bond donors.[18] The authors concluded that DESs are capable of introducing oxygen and nitrogen functional groups to the carbon surface at temperatures as low as 60 ^oC under sonication treatment. Amide-based DESs resulted the most effective variation in terms of graphene functionalization. In this work, we explore the use of DESs to modify commercial GFs to enhance their electrochemical activity and performance as electrodes in VRFBs.

Results and Discussion

The goal of this work was to develop a series of surface treatment methodologies for commercial GFs to increase their hydrophilicity, surface area and electrochemical activity towards V(IV)/V(V) and V(II)/V(III) redox reactions based on DES. In the last 10 years the application of DESs as electrolytes or/and redox-active materials for RFBs have been gradually gathering attention.[5a, 19] However, most efforts have been devoted to the electrolyte and the battery efficiency metrics. Here we study the impact of treating carbon electrodes with DES, which in turn can bring new understanding to the interaction of DES electrolytes and carbon electrode surfaces.

Several reports indicate that iron can work as a graphitization catalyst during the pyrolysis of precursors such as organic small-molecules,[20] polymers and bio-polymers.[21] Based on these findings, our hypothesis is that a type II DESs with $FeCl_3$ could induce a re-graphitization of the fibres, thus enhancing electronic conductivity and surface area. Additionally, iron-based treatments can produce etching on the carbon fibres and potentially, decoration of the fibres with iron oxide particles, which can act as catalytic sites for vanadium electrochemistry.[22] With this in mind, a type II DES composed of NH_4Cl and $FeCl_3$•$6H_2O$ (1.6:1) (melting point = 223 ^oC) ($NH_4Cl/FeCl_3$) was chosen for this study. Additionally, we hypothesized that type III DES could introduce oxygen and nitrogen functional groups into the carbon lattice, which could have a catalytic effect on vanadium electrochemistry. In previous work by Hayyan *et al*. on functionalization of graphene oxide using DESs, the authors concluded that samples exposed to choline chloride/urea (1:2) (ChCl/U) (melting point = 12 ^oC) DES under heating and sonication (sonothermal conditions) exhibited higher concentration of oxygen and nitrogen functional groups compared to other type III DESs based on polyols or organic acids as hydrogen bond donors.[18] Moreover, urea has been shown to enhance the activity of carbonaceous electrodes for V(II)/(VIII) electrochemical reactions.[10c] Because of this, ChCl/U was chosen as the prototypical type III DES for this study.

Table 1: Compendium of surface treatments studied herein.

Experiment	Step 1	Step 2
B1	No	No
B2	800 ^oC, 3 h, N_2r	No
B3	400 ^oC, 30 h, Air	No
GF1-L	250 ^oC, 3h, NH_4Cl/ $FeCl_3$	No
GF1-LH	250 ^oC, 3h, NH_4Cl/ $FeCl_3$	800 ^oC, 3 h, N_2
GF1-HL	800 ^oC, 3 h, N_2	250 ^oC, 3 h $NH_4Cl/FeCl_3$
GF2-L	60 ^oC, 3 h, ChCl/U	No
GF2-LH	60 ^oC, 3 h ChCl/U	800 ^oC, 3 h, N_2
GF2-HL	800 ^oC, 3 h, N_2	60 ^oC, 3 h, ChCl/U

GF1 stands for thermal treatment in NH4Cl/FeCl$_3$, GF2 stands for sonothermal treatment in ChCl/U. The secondary labels "L" or "H" refers to low or high temperature treatments and the order of application

The impact of these treatments on the chemical composition of GFs and their electrochemical properties were compared to other methodologies typically reported to increase performance of commercial GFs that involved thermal activation under N_2 atmosphere at 800 ^oC or oxidation at 400 ^oC under air, Table 1.[9b, 23] The surface modification methodologies were divided in two steps: low (L) or high (H) temperature treatments and a third step involving wash to remove any excess of DES. The low temperature treatments consisted in exposure of GFs to ChCl/U by sonication at 60 ^oC for 3h (sonothermal treatment) or to $NH_4Cl/FeCl_3$ at 250 ^oC for 3h (thermal treatment). The difference in temperature between the two lower temperature treatments was due to the melting point of $NH_4Cl/FeCl_3$ at 223 ^oC. The eutectic mixture should be above melting point to ensure uniform coverage of the GF. On the other side, performing the sonothermal treatment with ChCl/U at 250 ^oC was undesirable since the onset of thermal decomposition for this DES is 90 ^oC.[24] However, previous studies of the oxidation of carbon fibres showed that the optimum temperature for oxidating these materials with atmospheric air is of 400 ^oC for GFs and 475 ^oC for carbon paper.[9b, 23] At this temperature, the oxidation of the fibres will be mostly due to the corrosive effect of the Fe-based DES. The high temperature treatment consisted in a re-carbonization step at 800 ^oC for 3h under N_2 atmosphere in all cases. Samples treated thermally with $NH_4Cl/FeCl_3$ were labelled as **GF1-XY**, samples treated sonothermally with ChCl/U were labelled as **GF2-XY**, where "X and "Y" placeholders denote low or high temperature treatment and the order of application. A detailed procedure can be found in the experimental section. The GFs that served as benchmarks in this investigation were pristine felt "**B1**", thermally activated felt "**B2**" and oxidized felt "**B3**".

Surface analysis:

The surface chemical composition, area, and morphology of GFs for the different approaches were studied by x-ray photoelectron spectroscopy (XPS), scanning electron microscopy (SEM), Brunauer-Emmett-Teller surface area analysis (BET) drop shape analysis (DSA) and Raman spectroscopy.

The inert atmosphere thermal treatment was expected to increase the crystallinity of the graphitic fibres, whereas the oxidative treatment was expected to increase the number of defects on the graphite. According to BET analysis of the benchmarks, the thermal activation under inert atmosphere and the oxidative activation increased the surface area of samples **B2** and **B3** in 75% and 77% respectively *vs.* pristine felt **B1**, in agreement with previous reports on the surface oxidation of carbon paper (Figure 1a).[23] Sample **GF1-L**, which was treated with $NH_4Cl/FeCl_3$ DES without further carbonization steps, showed 67% higher surface area than **B1**, but slightly lower than benchmarks **B2** and **B3**. The introduction of a high temperature activation step promoted an increase in the surface area of samples **GF1-LH** and **GF1-HL** with respect to **GF1-L** of 12% and 46% respectively. Both samples also outperformed benchmarks **B2** and **B3**. Sample **GF1-LH**, which was re-carbonized in the presence of $NH_4Cl/FeCl_3$, resulted in an intermediate surface area, while **GF1-HL,** resulted in the highest surface area of the series. This observation suggests that our first hypothesis on the enhancement of the surface area due to iron-

catalysed re-carbonization of the fibres might be only partially correct as it was expected for **GF1-LH** to exhibit the largest surface area due to a re-carbonization step in the presence of $NH_4Cl/FeCl_3$. Therefore, other phenomena such as etching or oxidation of the fibres due to corrosion might have a major impact on the increasing of the surface area observed for GF1 series with respect to the benchmarks.

Samples sonicated in ChCl/U exhibited the largest surface area of the present study, with **GF2-HL** displaying the highest value, again showing that a re-carbonization step before the low temperature treatment promoted the largest surface areas (Figure 1a). The re-carbonization of the sample in the presence of the DES had a slightly negative impact on the surface area, compared to **GF2-L**, which was only treated with ChCl/U under sonothermal conditions. Similarly, as observed for GF1 series, the sample in which the high temperature treatment preceded the low temperature treatment exhibited the largest surface area. This suggests a synergistic effect between the formation of more crystalline graphitic fibres due to the inert thermal activation, and the low temperature treatments, which resulted in larger surface areas compared to experiments in which the re-graphitization takes places after the low temperature treatment or in which the low temperature treatment is applied directly to the pristine GF.

The average half pore width of the materials was also determined through BET analysis (Figure 1b). Sample **B3** exhibited the smallest pore size among benchmarks, which can be a consequence of microporosity generated by the etching of the fibres due to the oxidating conditions, whereas samples **B1** and **B2** resulted in similar pore sizes, which suggest that the re-carbonization step in N_2 atmosphere does not modify the porosity of the samples. Samples **GF1-L** and **GF2-HL** exhibited similar pore sizes as **B3**, which suggests these methodologies produced similar microporosity to the oxidative treatment. On the other hand, samples **GF1-HL**, **GF2-L**, and **GF2-LH** exhibited all similar values of pore size to the pristine material.

Raman analysis of band “D”, composed of vibrational modes related to disordered graphitized carbon domains and amorphous carbon; and band “G” associated to the tangential vibrational mode of the C(sp^2) hexagonal graphitic lattice, allows to develop a metric to compare the degree of defects present in the graphitic surface of the fibres, which consist in analysis of the D to G bands area ratio (Figure 1c).[25] As such, as expected, **B2** sample exhibited the lowest D to G ratio of the benchmarks, since it was re-carbonized, it was expected to obtain a more crystalline graphitic material. In contrast, **B3** was the benchmark material with the highest D to G ratio because of the formation of oxidated carbon, which translated into defects or amorphous domains. **GF1-L** and **GF-HL** were found to exhibit the same D/G ratio even though the second sample included a re-carbonization step in the presence of the iron-based DES. **GF1-HL** exhibited the highest D/G ratio of GF1 series, which could indicate larger etching of the fibres, but also presence of ionic compounds on the fibre surface.[25] In fact, iron oxide and chloride salts were detected adsorbed on the surface of **GF1-HL** by SEM micrographs (Figure 2f), contributing to its high D/G ratio.

Alongside the surface area results, this suggest that our hypothesis on the re-graphitization of the fibres to obtain new ordered graphitic domains catalyzed by iron is not the correct explanation for the increases in surface areas detected for GF1 series. Iron-catalyzed re-graphitization is discarded since this treatment did not involve a re-carbonization step after the low temperature treatment.

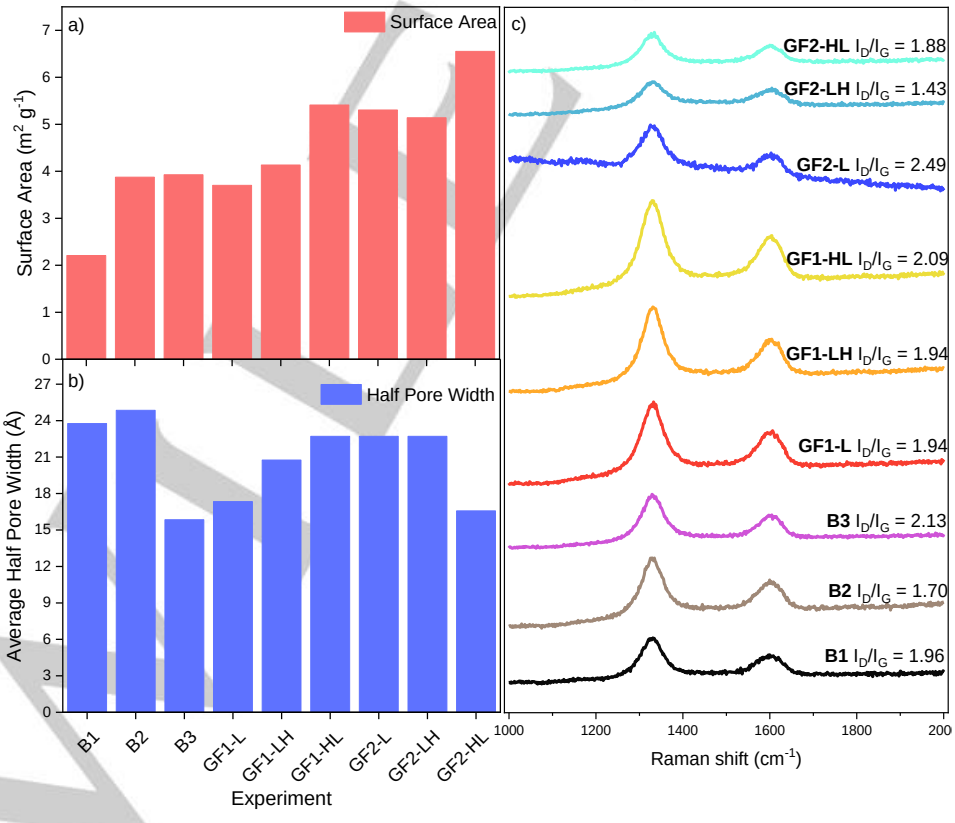

Figure 1: Analysis of the surface modification methodologies. a) Collection of BET surface area measurements of studied GFs. b) Collection of half-pore width BET estimations of studied GFs. c) Raman spectra highlighting D and G Raman bands and D/G ratios from studied samples

GF2-L exhibited the highest D/G ratio among the studied samples, while **GF2-LH** the lowest D/G ratio among studied samples and benchmarks, which would indicate that the low temperature treatment plus further carbonization of the felt in the presence of the organic components of the DES increased the degree of graphitization of the material. This suggest that any aliphatic groups introduced by the low temperature treatment were aromatized and incorporated into the graphitic lattice during the re-carbonization step.

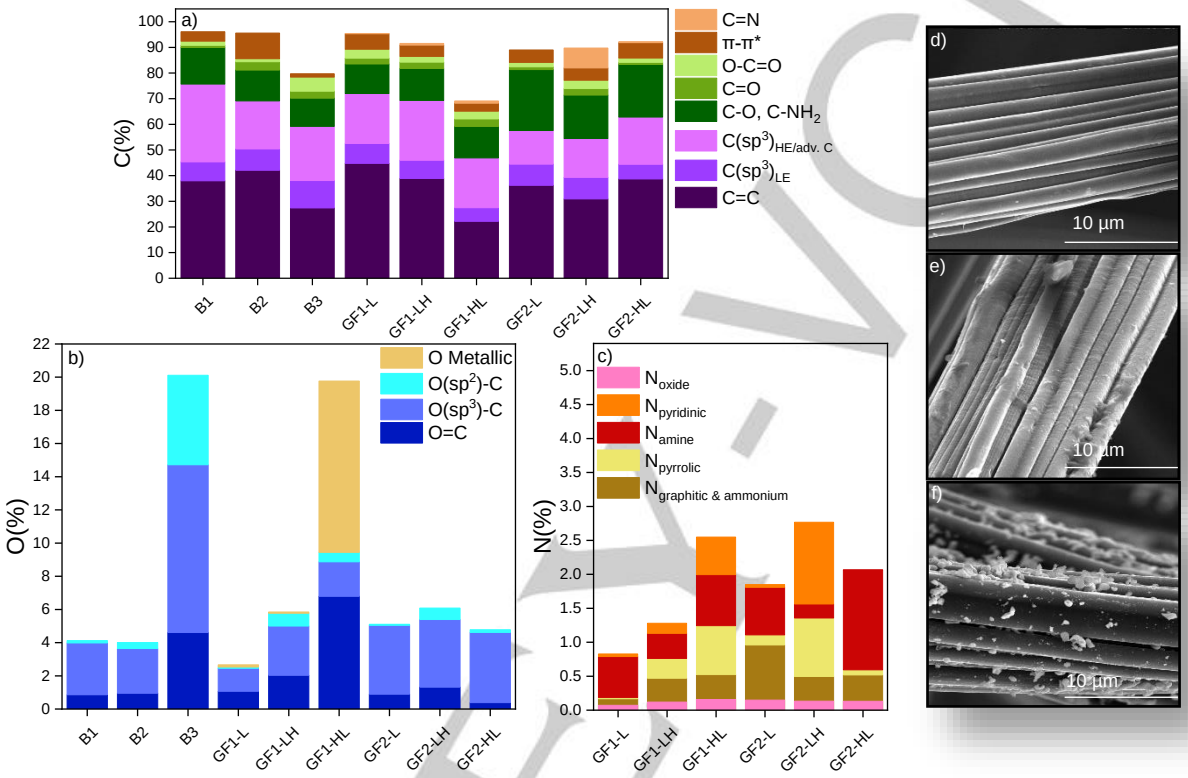

Figure 2: Stacked histograms representing the % of deconvoluted chemical environments contributing to the XPS high resolution spectra of a) C 1s, b) O 1s and c) N 1s of the studied samples. Secondary electron micrographs of d) **B1**, e) **B3** & f) **GF1-HL** felts

The deconvoluted chemical shift contributions to C 1s, O 1s and N 1s high resolution XPS spectra of all samples is shown in Figure 2a-c. A detailed compilation of numeric contributions to C, O, N, and Fe groups can be found in Table S1 in the supporting information document. The deconvoluted spectra of all samples can be found in Figures S1-S39 in the supporting Information document. The analysis of the benchmark samples revealed that the oxygen content of samples **B1** and **B2** was around 4%. The difference between the pristine and thermally activated samples relied on the nature of the oxygen-rich functional groups located on the fibres surface. In sample **B1**, aliphatic C-O contributions have a larger proportion, whereas in **B2**, aromatic C-O and ketone functionalities are slightly higher. Carboxylic contributions remained similar in both cases, probably due to the absence of an oxidative atmosphere. Moreover, the re-carbonized sample **B2** exhibited approximately 5% more contributions from C=C than pristine **B1**. On the other hand, the oxidized benchmark **B3** showed an increase up to 20% in oxygen content, with major contributions from carboxylic functional groups and aromatic C-O groups. The significative increase in oxygen content for **B3** caused roughness and corrosion on its surface, whereas that of **B1** is smoother, as can be appreciated in their SEM micrographs (Figures 2d-e). The proportion of ketone groups in **B3** remained similar to **B2**, which suggests that ketone groups start appearing at lower temperatures regardless of the atmosphere and remain constant despite increasing the temperature to 800 ºC.

XPS analysis of GF1 series revealed significant changes in the contributions from O and N functional groups depending on the sequence of treatments. Samples **GF1-L** and **GF1-LH** showed contributions of C=C peaks to C 1s band of 42% and 39% respectively, whereas **GF1-HL** showed a significantly smaller contribution. In this regard, SEM images of **GF1** series showed scarce deposition of Fe_2O_3 particles on the fibres for **GF1-L** and **GF1-LH**, (Figures S44 & S45 in the supporting information document). In contrast, **GF1-HL** exhibited higher amount of iron oxide coverage of the surface, with a Fe atomic content of 5.5% (Figure 2f). It is not clear why a carbonization pre-step as in **GF1-HL** would promote the incorporation of iron oxide particles onto the carbon surface compared to samples that involved a lower temperature treatment first as **GF1-L** or **GF1-LH**, and this will be further studied. The Fe_2O_3 particles confirmed by XPS and EDS (Figure 2f and Figures S49-S50 in the supporting information document) presented diameters in the range of 0.5-2 µm. They were firmly adsorbed to the fibres surface and tolerated the acidic washes. XPS revealed samples **GF1-L** and **GF1-HL** presented only 0.1 at% of Fe.

These observations were also correlated with a decrease in the contributions from aliphatic C-O functionalities for **GF1-HL** due to predominance of oxygen associated with iron oxide (metallic oxygen in Figure 2b). On the other side, **GF1-HL** showed higher contributions of C=O groups than **GF1-L** and **GF1-LH** according to their high-resolution O 1s spectra. Therefore, re-carbonizing the material in the presence of the iron-based DES, this is, after the low temperature treatment as in **GF1-LH**, reduced the population of ketone functionalities compared to first re-carbonizing the material and then applying the DES treatment. With regards to O-C=O contributions, **GF1-HL** exhibited the highest proportion, followed by **GF1-L**, similarly as observed for the ketone groups, which suggests that re-carbonizing the sample in the presence of DES had a negative impact on the carboxylic functionalities (the values of each functional group contribution can be found in Table S1 in the supporting information document). Regardless, all iron-treated samples showed higher proportions of C=O and O-C=O groups than the benchmark materials, excepting for the oxidised felt **B3**.

XPS analysis from GF2 series revealed that experiments **GF2-L** and **GF2-HL**, which had in common that no re-carbonization steps were applied after the low temperature treatment, resulted with the highest contributions from aliphatic C-O and C-N groups to the C 1s spectrum among studied samples. This result correlates with the previously discussed D/G ratio of **GF2-L**, which was significantly superior to all other studied samples, thus indicating that **GF2-L** was the sample with the largest amount of amorphous carbon due to functionalization with O and N groups. Therefore, these results suggest that our hypothesis on the introduction of heteroatomic functional groups to the carbon fibres due to the treatment with a urea-based DES was correct. Indeed, the sonothermal treatment functionalised the graphitic fibres to similar degree than the material obtained via oxidation treatment applied to sample **B3**.

XPS and Raman results that the low temperature treatment with ChCl/U impacts the proportion of heteroatoms decorating the surface, while the thermal activation impacts the graphitic ordering. It is noteworthy that although the sonothermal treatment with ChCl/U resulted effective for introducing aliphatic C-O and C-N groups onto the fibres surface, this treatment rendered similar proportions of ketone groups as the pristine benchmark, where even the samples which treatments involved a re-carbonization step resulted in lower C=O proportions than **B2** and **B3**. Therefore, this functionalization methodology does not alter the proportion of ketone groups. With regards to carboxylic groups, the sonothermal treatment resulted less effective than the oxidation benchmark **B3**, with only slight improvements with respect to **B1** and **B2**.

The analysis of N 1s spectrum showed that N-O functionalities remained relatively constant for all treatments. The atomic proportions of quaternary N species such as ammonium or graphitic nitrogen were higher in GF2 series compared to GF1 series, possibly due to the high concentration of choline chloride and urea in ChCl/U DES. Instead, GF1 series exhibited higher aliphatic nitrogen proportions. The thermally induced reaction of ammonium chloride into C-N groups is a possible explanation for this observation.

When comparing results from both GF1 and GF2 series, results showed that experiments in which the low temperature treatment was not followed by a re-carbonization step such as **GF1-L**, **GF1-HL**, **GF2-L** and **GF2-HL** had very low contributions from aromatic C-O, pyridinic and pyrrolic nitrogen functionalities and higher contributions from aliphatic groups. In contrast, experiments in which the low temperature treatment was followed by a re-carbonization step showed more contributions from aromatic O and N functional groups and a slight depletion of contributions from aliphatic groups, which suggest that the carbonization step modified the hybridization of the heteroatoms from sp^3 to sp^2. Also, C=O and O-C=O contributions were higher for GF1 series compared to GF2 series. Ketone and carboxylic contributions of samples **GF2-L** and **GF2-HL**, with no post-carbonization treatments resulted in lower atomic proportions than their counterparts treated with $NH_4Cl/FeCl_3$, whereas **GF2-LH** exhibited slightly higher ketone and carboxylic proportions than **GF1-LH**, which suggest that a re-carbonization in the presence of ChCl/U was more effective introducing these functional groups than the iron-based DES, whereas in treatments without post-carbonization, the iron-based DES introduced more of these functionalities, since the proportions of the samples treated with ChCl/U remained similar to the pristine benchmark. This could be a consequence of the corrosion effect of the iron-based DES due to the thermal treatment.

Table 2: Collection of contact angle results from modified samples

Experiment	Result (º)
B1	155.3
B2	146.4
B3	108.4
GF1-L	115.8
GF1-LH	125.6
GF1-HL	Hydrophilic
GF2-L	Hydrophilic
GF2-LH	125.1
GF2-HL	116.7

Finally, the hydrophilicity of the dried fibres prior to the electrochemical testing was studied by drop shape analysis (DSA) and water absorption experiments. Since GFs do not have a flat surface, the determination of the contact angle tends to be inaccurate, however, this experiment allowed us to compare the samples qualitatively. In water absorption experiments, the hydrophilic GFs absorb water and increase their density, therefore, they sink, whereas hydrophobic GFs remain on top. The contact angle values are displayed in Table 2, and photographs of the experiments are shown in Figure S. As expected, the contact angle measurements indicated that **B1** and **B2** were the most hydrophobic of the studied materials. Sample **B3** resulted in a considerable reduction of contact angle with respect to **B1**. However, in our hands, this GF behaved as a mildly hydrophilic material in DSA. The water absorption experiment showed the material remained floating after 30 min exposure to water. These results are in contrast with previous literature that reported that the thermal oxidation of GFs under atmospheric conditions at 400 ºC for 30h performed in here turned GFs into hydrophilic materials.[9b] Instead, it is in agreement with a recent report that also indicates this material is mildly hydrophilic, since no complete absorption of the water droplet was observed either.[26] Samples **GF1-L**, **GF1-LH**, **GF2-LH** and **GF2-HL** exhibited slightly less hydrophobic contact angles compared to **B1**, however these materials remained qualitatively hydrophobic after the treatments according to the drop shape analysis. The floating test experiments showed that samples **GF1-L** and **GF2-HL** were slightly immersed in the water layer, whereas samples **GF1-LH** and **GF2-LH** were clearly floating completely. These observations suggest that samples which underwent a re-carbonization step after the DES treatment resulted in more hydrophobic property than the rest. Finally, it was observed that samples **GF1-HL** and **GF2-L** were hydrophilic as the water drop was quickly absorbed by the felt, and the materials sank tin the water absorption experiment. This can be a consequence of the decoration of the fibres, since for **GF1-HL**, a high concentration of iron oxide particles and ionic species were detected on the surface, which can increase the hygroscopicity of the fibres. On the other hand, **GF2-L** resulted in the sample with the largest amount of ammonium N according to XPS, thus suggesting the presence of hygroscopic ionic compounds in the surface, most likely from the choline chloride.

To summarize the surface analysis section, it was found that the treatment of GFs with $FeCl_3/NH_4Cl$ DES increased the surface area of the materials, the ratio of amorphous to graphitic carbon and effectively introduced oxygen-based functional groups onto the carbon surface compared to the pristine material. Our results suggest that the larger surface areas observed for GF1 series are not due to an iron-catalysed re-graphitization of the materials, but to the

microporosity caused by the corrosive effect of the DES thermal treatment**.** Only the sample GF1-HL turned hydrophilic, due to the presence of oxide particles decorating the fibres, while the rest of the materials remained relatively hydrophobic. On the other hand, it was observed that the treatment with ChCl/U also increased the surface area of the materials. The sonothermal treatment was also effective at introducing both oxygen- and nitrogen-based functional groups onto the carbon surface. The hybridization of these heteroatoms depended on the order of the applied steps. The experiment in which the low temperature treatment was followed by the high temperature activation, was found to exhibit more aromatic functional groups and a lower ratio of amorphous to graphitic carbon than the rest of the samples. Therefore, this sequence of treatments improved the graphitization of the material through the aromatization of the introduced heteroatoms. GF2-L turned hydrophilic, and this was correlated with a higher proportion of ammonium N compared to rest of the GF2 samples. In the following section, the electrochemical performance of the modified materials will be discussed through the analysis of half-cell experiments.

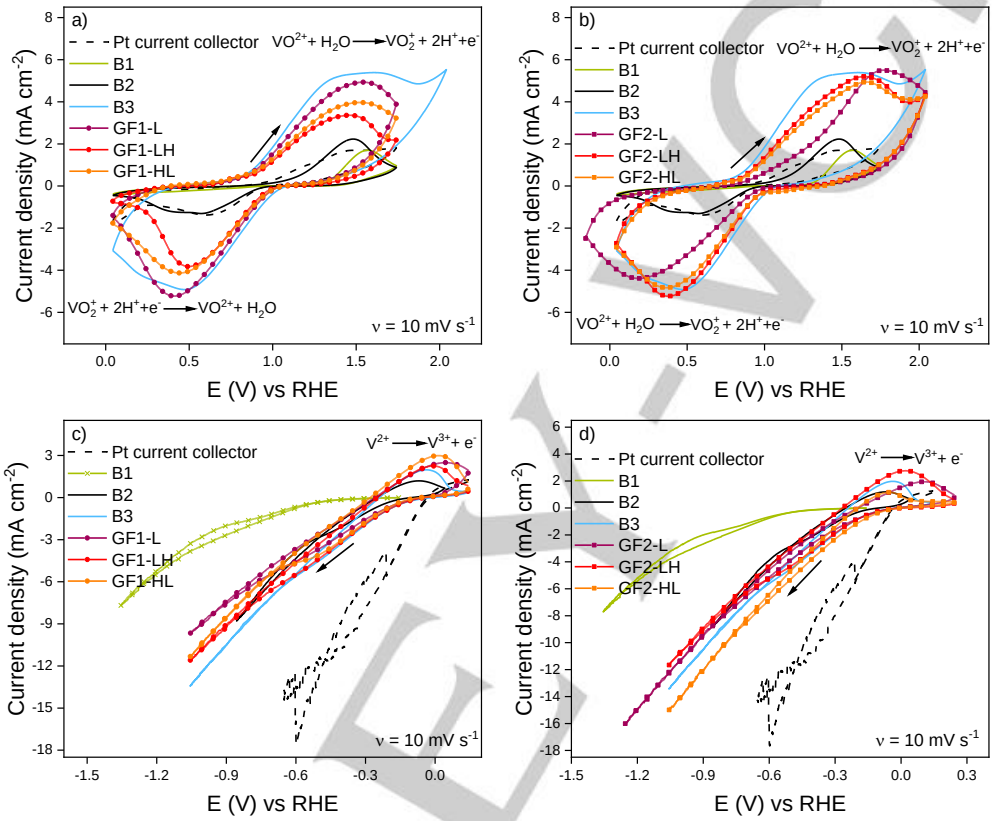

Figure 3: Cyclic voltammograms from benchmarks and treated samples. The exposed surface area of each sample was 2.513 cm^2. a & b) Experiments performed in 0.05 M $V^{3.5}$ solution. c & d) experiments performed in 0.05 M $V^{2.5}$ solution.

Half-cell analysis

Cyclic voltammetry (Figure 3) and impedance spectroscopy (Figure 4) were performed in a three-electrode electrochemical cell using the modified GFs as working electrodes to analyse the electrochemical activity towards V(IV)/V(V) and V(II)/V(III) redox pairs. The density current peak heights, Ip_a/Ip_c ratios and peak-to-peak separations in the cyclic voltammograms were used as metrics to determine effect of the treatments conducted with DESs on the electrochemical performance.

The oxidised felt **B3** demonstrated higher activity for the oxidation of **V**(IV) to V(V) **with** comparable current densities for the inverse electrochemical process than the GF1 series felts. On the other hand, all GF1 samples demonstrated moderate improvements compared to the oxidised sample **B3**, with similar peak-to-peak distances, but higher current densities. GF1 series of treated felts outperformed pristine and re-carbonized felts **B1** and **B2** for both oxidation and reduction reactions of VO^{2+}/VO_2^+, redox pair. The reduction of V^{3+} to V^{2+} appeared overshadowed by the hydrogen evolution reaction (HER) in GF1 series and **B2** and **B3** benchmarks due to these materials exhibiting more activity towards this parasitic electrochemical reaction than the pristine felt **B1**. However, the oxidation was more distinguishable in all cases, showing that all modified materials as well as the re-carbonized and oxidised benchmark materials had higher activity for V^{2+}/V^{3+} redox pair.

Within the same series, **GF1-L** showed the highest current densities of the studied samples for VO^{2+}/VO_2^+, redox couple, despite not being the felt with the largest surface area. However, its D/G ratio and C=C contribution to the C 1s XPS spectrum suggest that **GF1-L** was the sample with the highest degree of graphitization among the series, which can explain its better activity compared to **GF1-LH** and **GF1-HL** as an interplay between higher conductivities due to larger graphitic domains and presence of O and N functional groups as active sites for vanadium electrochemical reactions. **GF1-L** showed comparable activity to samples involving a re-carbonization step for the V^{2+}/V^{3+} redox couple, however, it also exhibited the lowest selectivity for hydrogen evolution reaction (HER) of the series, **B2** and **B3** benchmarks, which can help to increase lifetime of the all-vanadium redox flow battery by avoiding loses of electrolyte due to electrolysis at the operation potentials.

GF2 series felts outperformed **B1** and **B2** in terms of higher current densities for both oxidation and reduction reactions of VO^{2+}/VO_2^+, however, these

materials showed larger peak-to-peak distances than **B1** and **B2**, which translates to higher activation overpotentials.

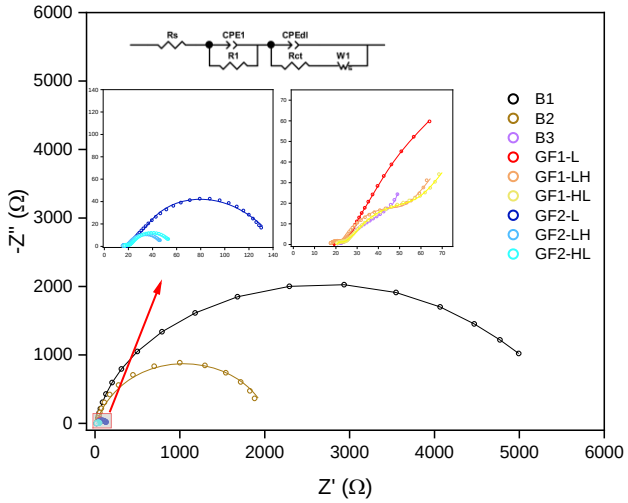

Figure 4: Nyquist impedance plots from benchmarks and treated GFs in 0.05 M $V^{3.5}$ solution. The exposed surface area of each sample was 2.513 cm^2. The circles represent the experimental data and the continuous line the fitted model.

Table 3: Collection of resistances obtained from circuit fitting.

Sample	Rs	Rct	R(Ws)
B1	24.6	4081.0	1471.0
B2	22.6	1566.0	466.0
B3	19.8	4.8	100.3
GF1-L	18.9	5.4	5.2
GF1-LH	17.4	4.7	24.8
GF1-HL	20.3	3.3	30.9
GF2-L	12.1	8.6	91.5
GF2-LH	14.7	6.6	22.7
GF2-HL	16.3	5.1	7.7

GF2-L exhibited the highest overpotentials for both oxidation and reduction reactions, as well as lower reduction current densities than samples involving a re-carbonization step. Samples **GF2-LH** and **GF2-HL** exhibited only moderate increases with respect to the benchmarks and higher reduction currents. The larger overpotentials and lower current densities observed for sample **GF2-L** can be associated with the fact that this material has the highest D/G ratio and proportion of O and N aliphatic groups of the studied samples. In this regard, sample **GF2-LH** resulted the best performing material of GF2 series, obtaining similar current densities and peak-to-peak distances as **B3** benchmark material. As such, for GF2 series, the best sample towards V(IV)/V(V) redox couple was also the one exhibiting the smallest surface area according to BET analysis, alongside important contributions from ketone and carboxylic functionalities, compared to other samples, in a similar fashion as for GF1 series. Nevertheless, as opposed to **GF1-L**, **GF2-LH** exhibited the lowest contribution from C=C of the series. **GF2** samples outperformed **B1**, **B2**, **B3** benchmarks with moderate increases in the current density of oxidation of V^{2+} to V^{3+}. **GF2-HL** showed the highest activity, characterized by large anodic current densities. Opposed to GF1 series, only **GF2-HL** exhibited slightly less selectivity for HER compared to **B2**, whereas **GF2-L** and **GF2-LH** exhibited similar or higher selectivity.

The impedance spectrum of the modified electrodes was obtained from three-electrode cell experiments by measuring the potential difference between the GFs acting as working electrodes and a silver/silver chloride reference electrode, to isolate impedance contributions coming from the working electrode. The Nyquist plots were composed by two regions of high and low frequencies. The high frequency segment was related to charge-transfer phenomena due to V(III)/V(IV) species at the electrode. The low frequency segment of the spectrum was related to mass-transfer phenomena within the porous of the electrode. For samples **B1**, **B2**, an equivalence circuit commonly used to describe porous carbonaceous electrodes was used to deconvolute ohmic, charge-transfer and mass-transfer contributions to the impedance spectrum.[27] In this circuit, a resistor modelling ohmic contributions (Rs) is connected to a parallel circuit featuring a CPE element to describe double layer capacitance phenomena on the electrode surface (CPEdl) and a series resistor modelling charge-transfer contributions (Rct) and a Warburg short element (Ws) to describe finite-length diffusion impedance, which includes a mass-transfer resistance component. For **B3**, GF1 series and GF2 series, it was necessary to add an additional RllCPE circuit (CPE1 and R1) to properly fit the equivalent circuit to the experimental data at high frequencies (Figure 4). This can suggest the presence of another charge-transfer/capacitive phenomenon at the electrode surface, taking place at similar frequencies, which could be caused by the functionalization and decoration of the fibres, which in cases like **B3** and **GF1-HL** can account for up to 20% of surface atomic composition according to XPS data. The numeric values obtained for the resistors can be consulted in Table 3.

Since all experiments were carried under the same conditions, the changes in Rs can be inversely correlated with the conductivity of the materials. Therefore, from the modified materials, **GF2-L** resulted the electrode with the highest conductivity, whereas **GF1-HL** and **B3** resulted the materials with the lowest conductivity. Since these materials showed the largest Raman I_D/I_G ratios and the largest heteroatomic surface compositions, the lower conductivity can be a consequence of the breaking of the graphitic domains.

The extracted charge-transfer resistances, which are related to the diameter of the high frequency arcs in the Nyquist plots, show that activating the GFs through a re-carbonization step as in the case of **B2,** certainly reduced the charge-transfer resistance and accelerate vanadium electrochemical kinetics at the electrode surface. However, there is a contrasting difference between samples **B1** and **B2** with samples **B3** and all modified GFs. This proved that the surface modification of the fibres, either by thermal oxidation or by the DES treatment improves the performance of the materials by sharply reducing the charge-transfer resistance associated to the vanadium electrochemical reactions. The significative reduction of the electrode's charge-transfer resistance unveils more subtle phenomena taking place at similar high frequencies. A possible explanation for the two charge-transfer/capacitive processes observed at high frequencies can be that the functionalization of the fibres was not homogeneous, therefore vanadium could be able to undergo its electron-transfer reactions with the heteroatoms or with carbon. The low frequency region of samples **B3**, **GF1-LH** and **GF1-HL** was characterized by a straight segment with a slope close 45° which was modelled as semi-infinite diffusion. Instead, the low frequency region of **GF1-L** showed the leftmost part of arc described by finite-length diffusional behaviour. The low frequency region of the GF2 series was described by a complete arc, equally modelled as finite-length diffusion impedance.

Full-cell analysis

The electrochemical active surface area of the materials was estimated by comparing the double layer capacitance of the materials against the specific capacitance of glassy carbon in 4 M H_2SO_4, (Figure 5 and Figures S51-S59 in the supporting information document). Although the active area values obtained by this methodology might not be exact due to obvious differences between glassy carbon and graphitic fibres, it produces a reference value that allows to compare our samples to each other. Previous BET measurements showed similar surface area values among studied benchmarks and samples regardless of the modification methodology. BET measurements also showed that samples which received a re-carbonization treatment followed by the lower temperature treatment such as **GF1-HL** and **GF2-HL** exhibited the largest surface areas of

their respective series, and that samples treated with ChCl/U had larger surface area than their counterparts treated with $NH_4Cl/FeCl_3$. On the other hand, ECSA measurements of the benchmarks showed that re-carbonizing the fibres under N_2 atmosphere (**B2** sample) promoted a 13-fold increase of active area with respect to the pristine sample **B1**, whereas the oxidation treatment promoted a 41-fold increase. In this regard, it has been pointed that the physical principle of N_2 physisorption in which BET methodology is based, is not sensible enough to probe very small microporosity caused by the surface methodologies, as an explanation for the disparity between BET surface areas and ECSA magnitudes.[28]

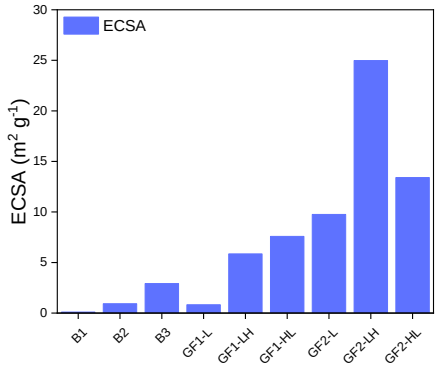

Figure 5: Electrochemical active surface area of benchmarks and treated samples.

Values for GF2 series were larger than GF1 series in agreement with BET. However, the sample with the largest active area was **GF2-LH** in which the re-carbonization treatment took place after the lower-temperature treatment. This was the expected observation, since we hypothesized that heating the fibres at high temperatures in the presence of the aliphatic groups introduced by the DES treatment, would promote the formation of new aromatic heterocyclic domains as well as defects. With regards to GF1 series, the results suggests that the largest increases in active area occurred between samples **GF1-LH** and **GF1-HL** against sample **GF1-L**, which suggest that for the samples treated with $NH_4Cl/FeCl_3$, the re-carbonization of the fibres play a major role in the increase of the active area, otherwise **GF1-L** would have exhibited a higher value.

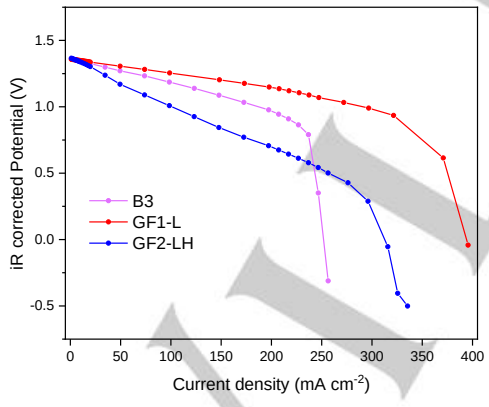

Figure 6: 50% SOC Discharge polarization curve analysis of best-performing samples at a flow rate of 30 mL min^{-1}

B3 was chose among the benchmark materials for full-cell analysis since it showed superior performance with respect to **B1** and **B2** in terms of vanadium (III and IV) electrochemical reversibility, as well as larger current density peaks and lower charge-transfer resistance. **GF1-L** was chosen among GF1 samples because it showed the largest current density peaks of reduction and oxidation for V(IV)/V(V), with comparable electrochemical reversibility to the other GF1 series samples and a larger current density peak for the oxidation of V(II)/V(III) than **B3** benchmark. **GF1-L** also exhibited the smallest selectivity for HER among its series. Nevertheless, it exhibited the largest charge-transfer resistance of its series according to EIS measurements, which suggest its performance is not fully optimized. **GF2-LH** was selected for full-cell analysis since it exhibited the best electrochemical reversibility for V(IV)/V(V) reaction and the second largest current density oxidation and reduction peaks. Moreover, it showed the largest V(II)/V(III) oxidation current density peak of its series, even larger than **B3** benchmark, and the smallest charge and mass transfer resistances of its series.

First, the contribution to losses in performance due to voltage drops during the discharge process of the three materials, was studied by discharge polarization curves (Figure 6). The battery was taken to 1.35 V (50% state of charge (SOC) open-circuit voltage (OCV) according Nernst equation) as starting point since at this SOC the battery offers a more representative picture of its discharge polarization.[23] An iR-corrected polarization curve is composed of three main regions, characterized by changes in the curve slope: low current densities (kinetic overpotential dominates), mid current densities (ohmic overpotential dominates) and high current densities (mass transport overpotential dominates).[29]

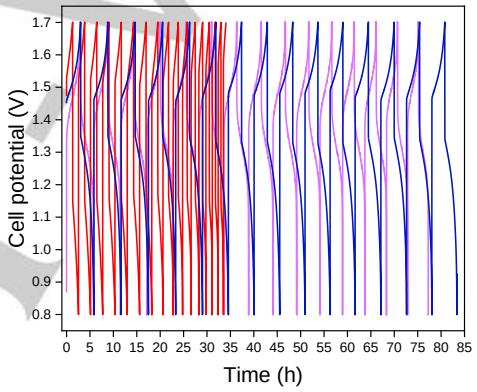

Figure 7: First 15 charge/discharge cycles of samples **B3** (lilac), **GF1-L** (red) and **GF2-LH** (blue) at 40 mA cm^{-2}

Kinetic loses are related to the activation energies of the vanadium electrochemical reactions on the carbonaceous surface. Ohmic loses are related to ionic resistances, electrode/electrolyte/membrane contacts and transport of the electroactive species within the electrode's pores. The ionic and contact resistances can be removed by performing an iR correction of the polarization curve by means of the high frequency resistance intercept of the battery, obtained through impedance measurements.[23, 29] Mass transport loses are related to the lack of availability of electroactive species from the bulk when the electrode is under high current.

The polarization curve in Figure 6 shows that all three electrodes exhibit small activation overpotentials, which is consistent with the half-cell impedance results and it is likely a consequence of the generation of new electroactive sites due to the increase of C-O and C-N functional groups on the electrode surface or the massive increase in active area evidenced by ECSA experiments. Since the cell potentials of the polarization curve were iR corrected, the ohmic losses are an indication of poor mass transfer of vanadium within the electrode pores. In this regard sample **GF1-L** exhibited less voltage drops than **B3** and **GF2-LH** and higher mass-transport limiting currents. The different onsets of the mass transport limiting currents of the three materials at same flow rates, are an indication of starvation of the electrode due to complete consumption of electrolyte. In this regard, the polarization curves suggest that **B3** had more electrochemical activity towards vanadium followed by **GF2-LH** and **GF1-L**. These results are in contrast with ECSA measurements which suggest an active area trend in the opposite order, however, would align with the oxygen content

observed by XPS analysis. It has been pointed that the enhancement of electrochemical activity of oxidated or functionalised carbon fibres can be a consequence of an increase of active area or oxygen- and nitrogen-rich groups bonded to the carbon surface.[9b, 23, 30] As such, in this case the trend observed for the mass limiting currents suggest it is the O and N content in the fibres surface and not the active area what is causing the increase of performance.

The galvanostatic charge/discharge curves of the first 15 cycles of samples **B3** and **GF2-LH** are displayed in Figure 7. Sample **GF1-L** was characterized by faster charge/discharge cycles compared to **B3** and **GF2-LH**. Since the polarization curve did not reveal significant overpotential fade at 40 mA cm^{-2}, then the material might be promoting side reaction with the electrolyte, which cause smaller energy efficiencies (EE) and accessible capacity (*vide infra*). Self-discharge reactions between Fe and V can be discarded as the presence of Fe in the sample after the treatments was negligible according to XPS. On the contrary, samples **B3** and **GF2-LH** were observed to have similar behaviour throughout the charge/discharge in the first cycles. However, **GF2-LH** was characterized by longer-periods of charge and discharge than **B3**. Moreover, slightly higher overpotentials can be appreciated at the onset of the charging and discharging plateaus for **GF2-LH** compared to **B3** in agreement with the obtained results for the polarization curves at low current densities.

For 1.35 M electrolyte, the battery theoretical volumetric capacity was 36.2 Ah L^{-1}. Therefore, for 25 mL tanks, the battery capacity was **905 mA h**. The samples efficiencies are displayed in Figure 8a while their capacity retention in Figure 8b All three samples were characterized by coulombic efficiencies (CE) between 93% and 98%. Sample **B3** was characterized by the highest EE of the three. **GF2-LH** showed approximately 10% less EE than **B3** which is a consequence of the sample exhibiting higher overpotentials for both charge and discharge processes. This causes less voltage efficiency and thus, lower energy efficiencies.

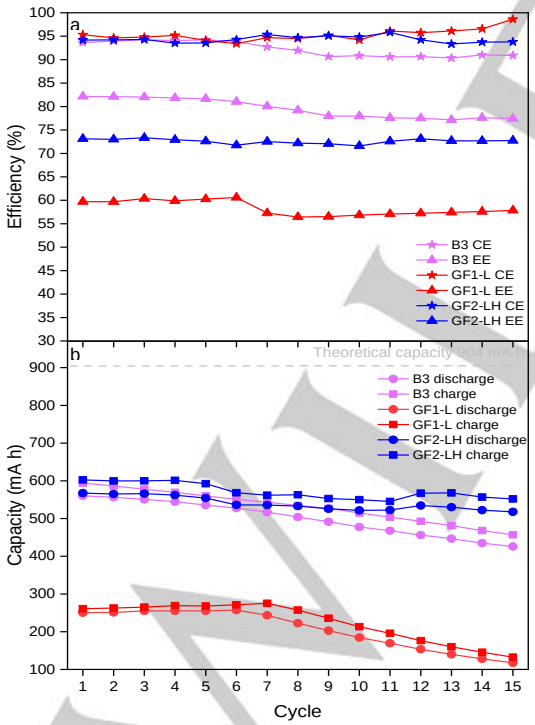

Figure 8: a) Full-cell configuration coulombic efficiencies (stars) and energy efficiencies (triangles) for benchmark **B3** (lilac), **GF1-L** (red) and **GF2-LH** (blue). b) Discharge capacity (circles) and charge capacity (squares) for the first 15 cycles.

The full-cell configuration with **GF1-L** electrode discharge capacity was observed to only reach approximately 26% of the theoretical capacity as exhibited in Figure 8b, which explains the shorter periods of activity observed in Figure 7. On the contrary, **B3** and **GF2-LH** discharge capacity was 65% of the available capacity during the first cycle despite exhibiting slightly larger overpotentials according to their polarization curves than **GF1-L**. This suggest that both materials are more selective towards vanadium reactions whereas **GF1-L** was more involved in other unwanted side reaction like hydrogen evolution due to electrolysis of the solvent. It was observed that sample **GF2-LH** exhibited better capacity retention than **B3** throughout the experiment, with **B3** suffering 25% of capacity fade after 15 cycles, whereas sample **GF2-LH** suffered 9% of capacity fade only. After the 15 cycles, the volume of the positive electrolyte was approximately 27 mL while the negative electrolyte 24 mL. This is caused by cross-over of the vanadium species from the negative towards the positive side, and solvent electrolysis on the negative side. Together, these phenomena caused changes in the electrolyte concentration and overall, loses in capacity.[31]

Although more studies are required to reduce the capacity fade observed for the material treated with ChCl/U, these results help to pave the way towards fully operative redox flow batteries working with type II or III DES-based electrolytes. If such a mild treatment as the one applied in this work was able to exert a dramatic improvement in electrochemical performance compared to the pristine material and higher capacity retention than the thermally oxidated felt **B3**, then it is likely that such battery electrodes will not even need any activation procedures. This because it is likely that the potentiostatic bias applied for the pre-charge step of the battery in the presence of the DES electrolyte will end up causing similar effects on the electrode surface as the one observed in this work. One of the key features of DES is their “designer” capability, which means that task-specific solvents can be prepared by modifying the nature of the mixture components. Therefore, a more optimised DES can potentially help to increase the energy efficiency of the battery by means of different surface-modification pathways.

Conclusion

Iron-based and urea-based DESs were involved in surface modification methodologies of graphite felts with the aim of improving their performance as electrodes for aqueous all-vanadium redox flow batteries. The surface chemistry of the materials and their electrochemical performance were compared against a pristine felt sample, a thermally activated sample, and an oxidated felt as benchmarks. As part of the methodology, the effect of the order of applying the DES treatments and carbonization steps in the surface chemistry and electrochemical activity of the materials was studied. It was observed that all treatments sharply increased the ECSA of the materials and introduced oxygen- and nitrogen-rich functional groups to the surface. All treated samples as well as the oxidated felt exhibited large increases of activity towards vanadium electrochemical reactions as characterized by larger current densities compared to the pristine and thermally activated felts, although the electrodes treated with ChCl/U resulted in slightly less electrochemically reversibility processes. Impedance spectroscopy analysis revealed that this is caused by a steep decrease in the charge-transfer resistance of the electrodes which can be a consequence of the materials now exhibiting larger active areas and more C-O and C-N groups. The graphite felt treated with ChCl/U and then carbonized resulted in the best performing sample in the full-cell configuration experiments, demonstrating comparable coulombic efficiencies and superior capacity retention to the thermally oxidated benchmark, but around 15% less energy efficiency, due to larger overpotentials as evidenced in the charge/discharge cycles and polarization experiments. These observations suggest that graphite electrodes used for batteries that work with DES-based electrolytes can be used without activation steps, thus saving costs, and making the system more sustainable.

Experimental Section

Preparation of deep eutectic solvents

All reagents involved in the preparation of DESs were purchased from Sigma-Aldrich UK and dried in a vacuum oven at 80 ºC for 12 h prior to their use.

ChCl/U: Choline chloride (34.2555 g, 0.25 mol, 1 eq.) and urea (29.4712 g, 0.49 mol, 2 eqs.) were ground together in a mortar until obtaining a homogeneous solid mixture. The mixture was then transferred to a round-bottom flask and heated at 80 ºC for 1 h under vigorous stirring. 50 mL of a colourless transparent liquid were obtained. The DES was stored under ambient atmosphere to let its moisture content to equilibrate with the environment.

$NH_4Cl/FeCl_3$: Iron (III) chloride hexahydrate (50 g, 0.19 mol, 1 eq.) and ammonium chloride (16 g, 0.3 mol, 1.57 eqs.) were ground together in a mortar until obtaining a homogeneous solid orange mixture.

Surface treatments

Re-carbonization step: Graphite felts were carbonized in a Carbolite Gero tubular furnace at 800 ºC for 3 h with a N_2 flux of 0.2 L min^{-1}.

Oxidation treatment: Graphite felts were heated in a Carbolite Gero tubular furnace at 400 ºC for 30 h with an air flux of 0.2 L min^{-1}.

$NH_4Cl/FeCl_3$ thermal treatment: approximately 5 g of NH_4Cl/Fe were spread on top and below a 20 cm^2 piece of GF until both sides of the felt were evenly covered by the salt. Then, the graphite felt piece was placed in a glass petri dish and heated at 250 ºC for 3h in a Thermo Scientific Heratherm furnace. Washing up: GFs were soaked in 30 mL of deionized water to remove the excess $NH_4Cl/FeCl_3$ prior to any high temperature treatment. If not high temperature treatment was applied, the felts were soaked in 5 mL of 5 M H_2SO_4, and this acid wash was repeated until visibly confirming that the washing solution was colourless. Usually this took between 5 or 7 washes. Then the felts were washed deionized water until the pH of the washing solution was between 6-7. The materials were dried at 80 ºC in a high-vacuum furnace for 12 h. The DES can be dried by distillation under vacuum in a rotary evaporator to be reutilized.

ChCl/U sonothermal treatment: A piece of 20 cm^2 of GF was suspended in 10 mL of DES in a beaker. The sample was then sonicated in an ultrasonic bath at 60 ºC for 3h. Washing up: GFs were taken out of the DES and washed with deionized water until the pH of the washing solution was between 6-7. The DES was stored and reutilized.

Surface characterization: Field emission scanning electron microscopy (SEM, FEI, Inspect F50) was used to analyze the morphology of the graphite felt electrodes. X-ray photoelectron spectroscopy (XPS, Thermo Scientific, Nexsa) was used to study the chemical composition of the fibres surface. Survey scans parameters: 50 eV pass energy, 10 scans, 50 s dwell time. C 1s, O 1s, N 1s, Cl 2p high resolution spectrum parameters: 50 eV pass energy, 30 scans, 50 s dwell time. Fe 2p high resolution parameters: 50 eV pass energy, 50 scans, 50 s dwell time. BET analysis were performed in a Nova Quantachrome instrument, using N_2 as adsorbate. Raman spectroscopy was performed using a Renishaw in Via instrument, equipped with a 660 nm laser. The spectra were obtained by performing 4 acquisitions with 30 s of exposure. Drop shape analysis was performed with a Kruss DSA 100 apparatus using deionized water, whereas for water absorption experiments GF samples of 0.5x0.5x0.3 cm were placed in a water vial and were left for 30 minutes before taking photographs.

Half-cell experiments

The experiments were carried out in a 5 mL glass cell. An Ag/AgCl electrode in saturated KCl was used as reference, a platinum coil as counter-electrode. The modified graphite felts were used as freestanding working electrodes. The materials were punched to obtain wafers of 1 cm diameter and 0.3 cm of thickness, approximately 2.51 cm^2 of area. The wafers were firmly held between two PTFE pieces, one of which had a rectangular Pt sheet of 0.917 cm^2 as current collector. The electrodes were carefully introduced in the electrolyte to avoid contact between the surface of the electrolyte and the Pt current collector. However, contact between the electrolyte and the Pt sheet due to capillarity of the felts is acknowledged, and CVs of the bare Pt current collector are included for comparison. For V(IV)/V(V) cyclic voltammetries and impedance measurements, the electrolyte was prepared by diluting a 1.6 M $V^{3.5}$ solution in 2 M H_2SO_4 and 0.5 M H_3PO_4 (Oxkem) to 0.05 M vanadium in deionized water. For V(II)/V(III) cyclic voltammetries, the electrolyte was prepared by electrochemically reducing a 1.35 M solution of vanadyl sulphate (Sigma-Aldrich) in 2.6 M H_2SO_4 to 0.5 M V(III) and 0.5 M V(III), named as $V^{2.5}$ and then diluting it to 0.05 M vanadium. The electrochemical impedance spectroscopy experiments were carried out potentiostatically with a potential amplitude of 10 mV around the open-circuit potential of $V^{3.5}$ solution, at frequencies between 0.1 Hz and 0.1 MHz with 10 points recorded per decade.

Full-cell experiments

The full-cell redox flow battery configuration involved metal plates, plastic separator sheets, metallic current collectors, graphite flow plates, PTFE electrode holders, electrodes, a membrane, and the electrolytes. The battery assembly consisted in using screws to apply 3.5 lbf•ft pressure in a radial way to make sure the compression was uniform. Afterwards the tubing was connected to the inlets and outlets of the battery onto the electrolyte tanks. To pump the electrolyte through the system a peristaltic pump was used with a rate of 30 mL min^{-1}. The catholyte was filled with 50 mL of a 1.35 M $VOSO_4$ 97% (Sigma Aldrich) solution in 2.6 M H_2SO_4, while the anolyte was filled with 25 mL of the solution. The electrolyte was precharged galvanostatically to 1.8 V and then potentiostatically at 1.8 V until the current dropped below 4 mA cm^{-2}, at this point the colour of the posolyte was yellow and the colour of the negolyte was purple. Before the experiments, 25 mL of catholyte were removed to balance the capacity with the anolyte. The electrolyte was degassed with nitrogen for 15 minutes prior use to avoid self-oxidation of the anolyte. The electrolyte was pumped for 30 minutes prior the beginning of the test to allow the electrode to be fully permeated and to encounter any possible leak. Nafion 115 was used as membrane and was activated according to the literature procedure.[32] Briefly: the membrane was boiled in H_2O_2, then washed with deionized water, then immediately soaked in 1 M H_2SO_4 and finally left in deionized water for 1 h.

The ECSA of the electrodes was estimated in single-cell configuration, following a literature procedure.[33] Briefly, 2 M H_2SO_4 aqueous solution was circulated through both cathode and anode, CV experiments were performed with 0.4 V windows at potentials were faradaic processes do not take place, to isolate non-faradaic contributions to the current at 5, 10, 20, 50, 100, 150, 200 mV s^{-1} scan rates. The average current at the mean potential was plotted against the scan rate and the data fitted linearly to obtain the electrode capacitance as the slope of the fitted curve. The ECSA calculated according to ECSA = C/C_s, where C_s is the specific capacitance of glassy carbon in 4 M H_2SO_4.

Acknowledgements

AJS, LMMH and MWT acknowledge the support from the UKRI Future Leaders Fellowship (). AJS acknowledges the Farady Institution (EP/S003053/1) for funding under the SEED grant FIRG047.

Keywords: Graphite felt, carbon electrode, vanadium, redox flow battery, deep eutectic solvent.

[1] a) K. E. Rodby, T. J. Carney, Y. Ashraf Gandomi, J. L. Barton, R. M. Darling, F. R. Brushett, *J. Power Sources* **2020**, *460*, 227958-227969 ; b) G. Kear, A. A. Shah, F. C. Walsh, *Int. J. of Energy Res.* **2012**, *36*, 1105-1120; c) X. Z. Yuan, C. Song, A. Platt, N. Zhao, H. Wang, H. Li, K. Fatih, D. Jang, *Int. J. of Energy Res.* **2019**, *43*, 6599-6638; d) M. Zhang, M. Moore, J. S. Watson, T. A. Zawodzinski, R. M. Counce, *J. Electrochem. Soc.* **2012**, *159*, A1183-A1188.

[2] a) S. Rudolph, U. Schröder, I. M. Bayanov, *J. Electroanal. Chem.* **2013**, *703*, 29-37; b) J. Noack, N. Roznyatovskaya, T. Herr, P. Fischer, *Angew. Chem. Int. Ed.* **2015**, *54*, 9776-9809.
[3] a) M. Gencten, Y. Sahin, *Int. J. Energy Res.* **2020**, *44*, 7903-7923; b) A. Forner-Cuenca, F. R. Brushett, *Curr. Opin. Electrochem.* **2019**, *18*, 113-122.
[4] P. Qian, H. Zhang, J. Chen, Y. Wen, Q. Luo, Z. Liu, D. You, B. Yi, *J. Power Sources* **2008**, *175*, 613-620.
[5] a) Q. Wang, Z. G. Qu, Z. Y. Jiang, W. W. Yang, *Appl. Energy* **2018**, *213*, 293-305; b) W. Wang, Q. Luo, B. Li, X. Wei, L. Li, Z. Yang, *Adv. Funct. Mater.* **2013**, *23*, 970-986.
[6] J. P. V. Tafoya, M. Thielke, G. Tian, R. Jervis, A. B. J. Sobrido, *Curr. Opin. Chem. Eng.* **2022**, *38*, 100876-100885.
[7] K. J. Kim, H. S. Lee, J. Kim, M. S. Park, J. H. Kim, Y. J. Kim, M. Skyllas-Kazacos, *ChemSusChem* **2016**, *9*, 1329-1338.
[8] a) L. Eifert, R. Banerjee, Z. Jusys, R. Zeis, *J. Electrochem. Soc.* **2018**, *165*, A2577-A2586; b) Y. Lv, C. Han, Y. Zhu, T. Zhang, S. Yao, Z. He, L. Dai, L. Wang, *J. Mater. Sci. Technol.* **2021**, *75*, 96-109; c) Y. Jiang, Z. Liu, Y. Lv, A. Tang, L. Dai, Z. He, *Chem. Eng. J.* **2022**, *443*, 136341-136349.
[9] a) K. V. Greco, A. Forner-Cuenca, A. Mularczyk, J. Eller, F. R. Brushett, *ACS Appl. Mater. Interfaces* **2018**, *10*, 44430-44442; b) B. Sun, M. Skyllas-Kazacos, *Electrochim. Acta* **1992**, *37*, 1253-1260.
[10] a) Y. Shao, X. Wang, M. Engelhard, C. Wang, S. Dai, J. Liu, Z. Yang, Y. Lin, *J. Power Sources* **2010**, *195*, 4375-4379; b) Z. He, L. Shi, J. Shen, Z. He, S. Liu, *Int. J. Energy Res.* **2015**, *39*, 709-716; c) Y. Jian, M. Du, G. Cheng, P. Gao, T. Dong, J. Zhou, X. Feng, Z. He, Y. Li, L. Dai, W. Meng, L. Wang, *J. Energy Chem.* **2021**, *59*, 706-714.
[11] R.-H. Huang, C.-H. Sun, T.-m. Tseng, W.-k. Chao, K.-L. Hsueh, F.-S. Shieu, *J. Electrochem. Soc.* **2012**, *159*, A1579-A1586.
[12] K. J. Kim, M. S. Park, J. H. Kim, U. Hwang, N. J. Lee, G. Jeong, Y. J. Kim, *Chem. Commun.* **2012**, *48*, 5455-5457.
[13] F.-j. Zhang, H.-t. Zhang, *New Carbon Materials* **2021**, *36*, 82-92.
[14] M. W. Thielke, G. Tian, A. Jorge Sobrido, *JPhys. Mater.* **2022**, *5*, 24004-24019.
[15] T. Welton, *Green Chem.* **2008**, *10*, 483-183.
[16] M. Deetlefs, K. R. Seddon, *Green Chem.* **2010**, *12*, 17-30.
[17] E. L. Smith, A. P. Abbott, K. S. Ryder, *Chem. Rev.* **2014**, *114*, 11060-11082.
[18] M. Hayyan, A. Abo-Hamad, M. A. Alsaadi, M. A. Hashim, *Nanoscale Res. Lett.* **2015**, *10*, 1-26.
[19] a) D. Lloyd, T. Vainikka, K. Kontturi, *Electrochim. Acta* **2013**, *100*, 18-23; b) M. H. Chakrabarti, F. S. Mjalli, I. M. AlNashef, M. A. Hashim, M. A. Hussain, L. Bahadori, C. T. J. Low, *Renewable and Sustainable Energy Rev.* **2014**, *30*, 254-270; c) B. Chakrabarti, J. Rubio-Garcia, E. Kalamaras, V. Yufit, F. Tariq, C. T. J. Low, A. Kucernak, N. Brandon, *Batteries* **2020**, *6*, 38; d) Y. Wang, H. Zhou, *Energy Environ. Sci.* **2016**, *9*, 2267-2272; e) Q. Xu, L. Y. Qin, Y. N. Ji, P. K. Leung, H. N. Su, F. Qiao, W. W. Yang, A. A. Shah, H. M. Li, *Electrochim. Acta* **2019**, *293*, 426-431; f) Q. Ma, L. Zhao, J. Xu, H. Su, W. Zhang, Q. Xu, *Electrochim. Acta* **2020**, *353*, 136486-136502; g) M. E. Di Pietro, A. Mele, *J. Mol. Liq.* **2021**, *338*, 116597-116627.
[20] a) J. Yang, S. Zuo, *Diamond Relat. Mater.* **2019**, *95*, 1-4; b) M. Sevilla, C. Sanchís, T. Valdés-Solís, E. Morallón, A. B. Fuertes, *Carbon* **2008**, *46*, 931-939.
[21] a) R. D. Hunter, J. Ramirez-Rico, Z. Schnepp, *J. Mater. Chem. A* **2022**, *10*, 4489-4516; b) K. Lotz, A. Wütscher, H. Düdder, C. M. Berger, C. Russo, K. Mukherjee, G. Schwaab, M. Havenith, M. Muhler, *ACS Omega* **2019**, *4*, 4448-4460; c) X. Zhang, Q. Yan, J. Li, I. W. Chu, H. Toghiani, Z. Cai, J. Zhang, *Polymers* **2018**, *10*, 183.
[22] L. Xia, T. Long, W. Li, F. Zhong, M. Ding, Y. Long, Z. Xu, Y. Lei, Y. Guan, D. Yuan, Y. Zhang, C. Jia, L. Sun, Q. Sun, *Small* **2020**, *16*, 2003321-2003331.
[23] K. V. Greco, A. Forner-Cuenca, A. Mularczyk, J. Eller, F. R. Brushett, ACS *Appl. Mater. Interfaces* **2018**, *10*, 44430-44442.
[24] M. Gilmore, S.-K. Malgorzata, J. D. Holbrey, *J. Chem. Eng. Data* **2019**, *64*, 5248-5255.
[25] M. W. Thielke, S. Lopez Guzman, J. P. Victoria Tafoya, E. García Tamayo, C. I. Castro Herazo, O. Hosseinaei, A. Jorge Sobrido, *Front. Mater.* **2022**, *9*, 1-10.
[26] A. Kaur, K. I. Jeon, S. S. Kim, J. W. Lim, *Compos. Struct.* **2022**, *290*, 115546-115548.
[27] a) A. Forner-Cuenca, E. E. Penn, A. M. Oliveira, F. R. Brushett, *J. Electrochem. Soc.* **2019**, *166*, A2230-A2241; b) E. B. Boz, P. Boillat, A. Forner-Cuenca, *ACS Appl. Mater. Interfaces* **2022**, *14*, 41883-41895.
[28] a) A. M. Pezeshki, J. T. Clement, G. M. Veith, T. A. Zawodzinski, M. M. Mench, *J. Power Sources* **2015**, *294*, 333-338; b) T. J. Rabbow, A. H. Whitehead, *Carbon* **2016**, *111*, 782-788.
[29] D. Aaron, Z. Tang, A. B. Papandrew, T. A. Zawodzinski, *J. Appl. Electrochem.* **2011**, *41*, 1175-1182.
[30] K. J. Kim, H. S. Lee, J. Kim, M.-S. Park, J. H. Kim, Y.-J. Kim, M. Skyllas-Kazacos, *ChemSusChem* **2016**, *9*, 1329-1338.
[31] Q. Luo, L. Li, W. Wang, Z. Nie, X. Wei, B. Li, B. Chen, Z. Yang, V. Sprenkle, *ChemSusChem* **2013**, *6*, 268-274.
[32] B. Jiang, L. Yu, L. Wu, D. Mu, L. Liu, J. Xi, X. Qiu, ACS *Appl. Mater. Interfaces* **2016**, *8*, 1228-12238.
[33] R. R. Jacquemond, C. T.-C. Wan, Y.-M. Chiang, Z. Borneman, F. R. Brushett, K. Nijmeijer, A. Forner-Cuenca, *Cell Rep. Phys. Sci.* **2022**, *3*, 100943-100968.

Entry for the Table of Contents

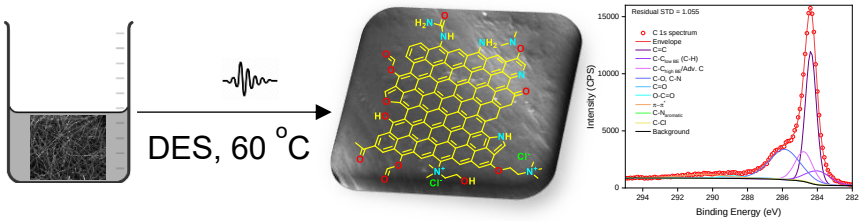

Methodologies were developed to treat graphite felts with deep eutectic solvents (DES) to increase their performance as electrodes for all-vanadium flow batteries. All materials exhibited significantly lower charge-transfer resistances and higher electrochemical activity for vanadium reactions compared to the pristine material. An electrode activated with a urea-based DES showed comparable efficiencies and superior capacities than an oxidatively activated electrode used as benchmark.